Iraqi Journal of Physics, 2024
https://doi.org/10.30723/ijp.v22i4.1320
Vol. 22, No. 4, PP. 139-147
P-ISSN: 2070-4003
E-ISSN: 2664-5548

Electrospun PAN@Ferrites Nanofibers for Rectifier and Humidity Devices

Ban Abbas Rijah[1a*] and Iftikhar M. Ali [1b]
[1]*Department of Physics, College of Science, University of Baghdad, Baghdad, Iraq*
[a*] Corresponding author: banabaas236@gmail.com

Abstract

Zinc cobalt ferrite ($ZnCoFe_2O_4$) and zinc ferrite ($ZnFe_2O_4$) were prepared using the sol-gel synthesis. Composite materials, PAN@$CoFe_2O_4$ and PAN@$ZnCoFe_2O_4$, were created by combining polyacrylonitrile (PAN) polymer with $ZnCoFe_2O_4$ and $ZnFe_2O_4$. Electrospinning was used to apply thin coatings onto glass and p-Si wafers. The synthesized fibre for both pure PAN polymers and their ferrite-based composites was illustrated in Field Emission Scanning Electron Microscopy (FESEM) images. The X-ray diffraction (XRD) analysis reveals that the PAN polymer exhibits a prominent peak at a precise angle of 29. 3345°.The size of this peak remains constant in PAN composites containing ZnCoFe2O4 and CoFe2O4. Fourier transformer infrared (FTIR) shows that absorptions have stretching vibrations between metal and oxygen. Nanofiber composites display non-ohmic characteristics, as evidenced by current-voltage (I-V) tests. PAN nanofibers display conductive properties, whilst their ferrite composites demonstrate rectification behaviour at room temperature when subjected to a low applied field. For PAN NFs, there is no effect when relative humidity percentage increases and decreases, but with adding ferrite materials PAN@$ZnFe_2O_4$ and PAN@$ZnCoFe_2O_4$ where, there is a significant change in resistance when humidity increases and decreases.

Article Info.

Keywords:
Humidity Sensors, $ZnCoFe_2O_4$, $ZnFe_2O_4$, PAN Nanofibers, Electrospinning.

Article history:
Received: Jun. 13, 2024
Revised: Sep. 01, 2024
Accepted: Sep.23, 2024
Published:Dec.01,2024

1. Introduction

In 1996, an initial investigation was carried out on the production of polyacrylonitrile (PAN) nanofibers (NF) using electrospinning [1]. Previous publications on electrospinning and its many uses have included many incisive evaluations [2-4]. Subsequently, this technique was widely used by researchers, mainly when PAN was used as a precursor [5-8], and medical equipment [9]. Another example is an antiviral agent incorporated into surgical gowns and facemasks, as well as other personal protective equipment, composed of nanocomposites such as PAN polymers, ZnO nanoparticles, and Viroblock [10]. This agent is favoured due to its high boiling point, strong conductivity, low viscosity, excellent solubility, and wide availability.

Dimethylformamide (DMF) is a polar organic solvent used in various chemical and industrial applications. It is most often used to dissolve and electro spin PAN [11]. The characteristics of the nanofibers may be impacted by the molecular weight of the PAN. Lower mechanical strength and thermal stability nanofibers may be produced using low-molecular-weight PAN [12]. On the other hand, PAN with a greater molecular weight may produce nanofibers with improved mechanical and thermal stability properties [13]. For electrospinning PAN nanofibers, the optimal flow rate varies depending on the specific processing parameters and is between 0.1 and 2 $mL.h^{-1}$. Low production rates might result from insufficient electrostatic force to extract the polymer solution from the spinneret tip at lower flow rates [14]. While electrospinning may seem simple, many variables impact the final electro spun. NFs are fibres that have dimensions on the nanoscale, making them exceedingly fine

morphologies, including factors such as the solution, processing, and ambient conditions [15]. PAN fibrils have a periodic structure along their axis and a diameter of 8–10 nm [16]. PAN, DMSO, and H_2O theoretical ternary phase diagrams were created by Mo et al. [17]. Feng and Li demonstrated how wet-spinning PAN fibres alter their form when exposed to H_2O [18].

Humidity sensors have been the subject of much study recently due to their wide range of applications, making them increasingly significant to academics. The storage and food industries, mobile device electronics, weather forecasting, civil engineering, air conditioning buildings, healthcare, automotive, paper, medical, textile, pharmaceutical, and agricultural environment monitoring are just a few of the many industries that use humidity sensors. In industrial operations, gas sensors must be very reliable in detecting humidity differences down to the lowest amount [19, 20]. Humidity sensors' overall performance is often correlated with the physical, chemical, and microstructural properties of the sensing material employed in their creation [21]. Moreover, research has shown that basic specifications characterise an excellent humidity sensor, including short response and recovery time, high sensitivity, long stability, low hysteresis, repeatability, and remarkable linearity [22]. Based on their functions, several types of polymeric humidity sensors are classified, including capacitive, gravimetric, optical, and resistive types [23]. The advantages of capacitive-type sensors over resistive-type sensors are their low power consumption, good linear performance, simplicity of manufacture, and flexibility in accommodating downsizing and mobility [24]. The primary principle of operation for capacitive-type sensing relies on the change of capacitance, which dependents on the hygroscopic permittivity of the material, which varies in response to relative humidity [25].

The aim of this study is to create and examine composite materials by combining PAN polymer with zinc cobalt ferrite ($ZnCoFe_2O_4$) and zinc ferrite ($ZnFe_2O_4$). The main focus is to examine the structural and electrical properties of these materials, with particular attention on their non-ohmic behaviour and rectification characteristics in nanofiber composites.

2. Experimental Work

The electrospinning technique was used to generate PAN nanofibers, with and without the inclusion of ferrite nanostructures. PAN@ferrite composites were formed by incorporating ferrite nanoparticles into PAN nanofibers. The precursor solutions were made by dissolving 0.65 g of PAN polymer (with an average molecular weight of 150,000 g/mol and a purity of ≥ 99%) in 6 ml of DMF and then swirling the mixture magnetically for two hours until a uniform and transparent solution was obtained. Two PAN@ferrite composites were prepared by attaching 0.065 grams of $ZnFe_2O_4$ and $ZnCoFe_2O_4$ to the polymer solution. Fig. 1 illustrates the electrospinning process, which was carried out with a separation distance of 8 cm between the needle tip and the collector while applying a voltage of 15 kV.

For preparation of $ZnFe_2O_4$, 1.94 g of ferric chloride and 1.78 g of zinc nitrate were dissolved separately in two beakers, in 30ml distilled water. The solutions were then mixed individually using a magnetic stirrer for 10 minutes. The iron chloride solution was subsequently introduced into the zinc nitrate solution, accompanied by incessant agitation to guarantee thorough solubilisation, resulting in a 60 ml amalgamated solution. After stirring for an additional 15 minutes, ammonia was added to modify the pH to 9, creating an alkaline environment. The resultant solutions were applied onto glass slides and subjected to a temperature of 80°C for three hours, causing the liquid to evaporate and the samples to totally desiccate into a powdered form. The powder was then subjected to calcination in an oven at a temperature of 500°C for two

hours. Upon reaching room temperature, the samples were pulverised into a fine powder for subsequent utilisation.

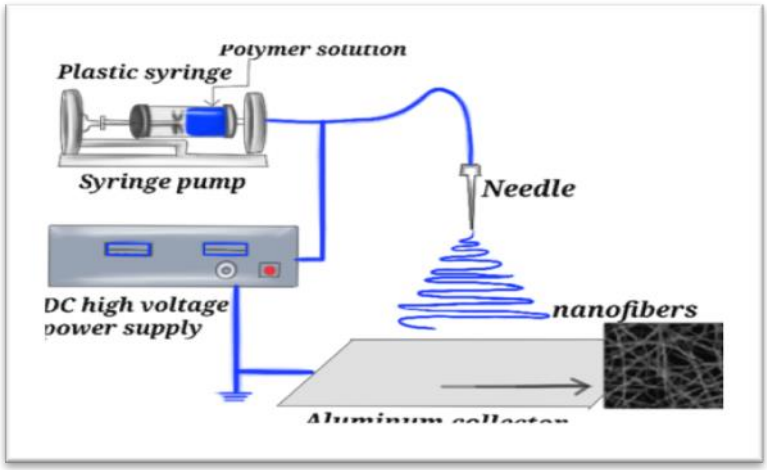

Figure 1: Design for the electrospinning apparatus assembly [26, 27].

3. Results and Discussion

Fig. 2 depicts the XRD patterns of pure PAN NFs, PAN@$ZnFe_2O_4$, and PAN@$ZnCoFe_2O_4$ composites. The XRD pattern of pure PAN nanofibers displayed a prominent peak at 2θ=29°, matching to the (221) diffraction plane, signifying the presence of crystalline structures in the synthesised polymers. The XRD pattern of the PAN@$ZnFe_2O_4$ composites exhibited a peak with an intensity of 1000 at 2θ = 29.93°, corresponding to the (202) diffraction plane, in accordance with card number (96-156-7174). Upon the amalgamation of $ZnCoFe_2O_4$ with PAN, a cubic structure was discerned, with the XRD pattern revealing a significant peak at 2θ = 29.56°, corresponding to the (202) diffraction plane, which fits with card number (96-900-5114). The patterns illustrate the interaction of PAN in a solution containing 0.065 M of $ZnFe_2O_4$ and $ZnCoFe_2O_4$, resulting in the creation of a cubic structure. The crystallite size (D) was determined utilising the Scherrer equation [28, 29]

$$D = K\frac{\lambda}{\beta \cos\theta} \qquad (1)$$

The trend of the average crystallite size during the sol-gel process is illustrated.

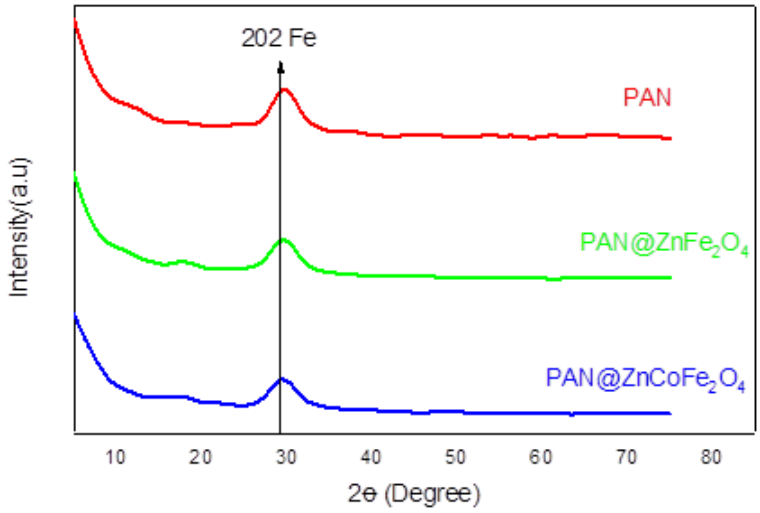

Figure 2: XRD pattern of PAN NFs, PAN@$ZnFe_2O_4$, and PAN@$ZnCoFe_2O_4$.

The determined average crystallite sizes for PAN@$ZnFe_2O_4$ and PAN@ $ZnCoFe_2O_4$ composites were 39.73 nm and 30.74 nm, respectively.

The composites nanofibers' morphological features were examined using filed emission scanning electron microscopy (FESEM). The FESEM images of the collected fibres are shown in Fig. 3. The electrospinning parameters that produced the soft polymeric nanofibers were identified by morphological research. Nanofiber diameter is shown in the inset of Fig. 3.

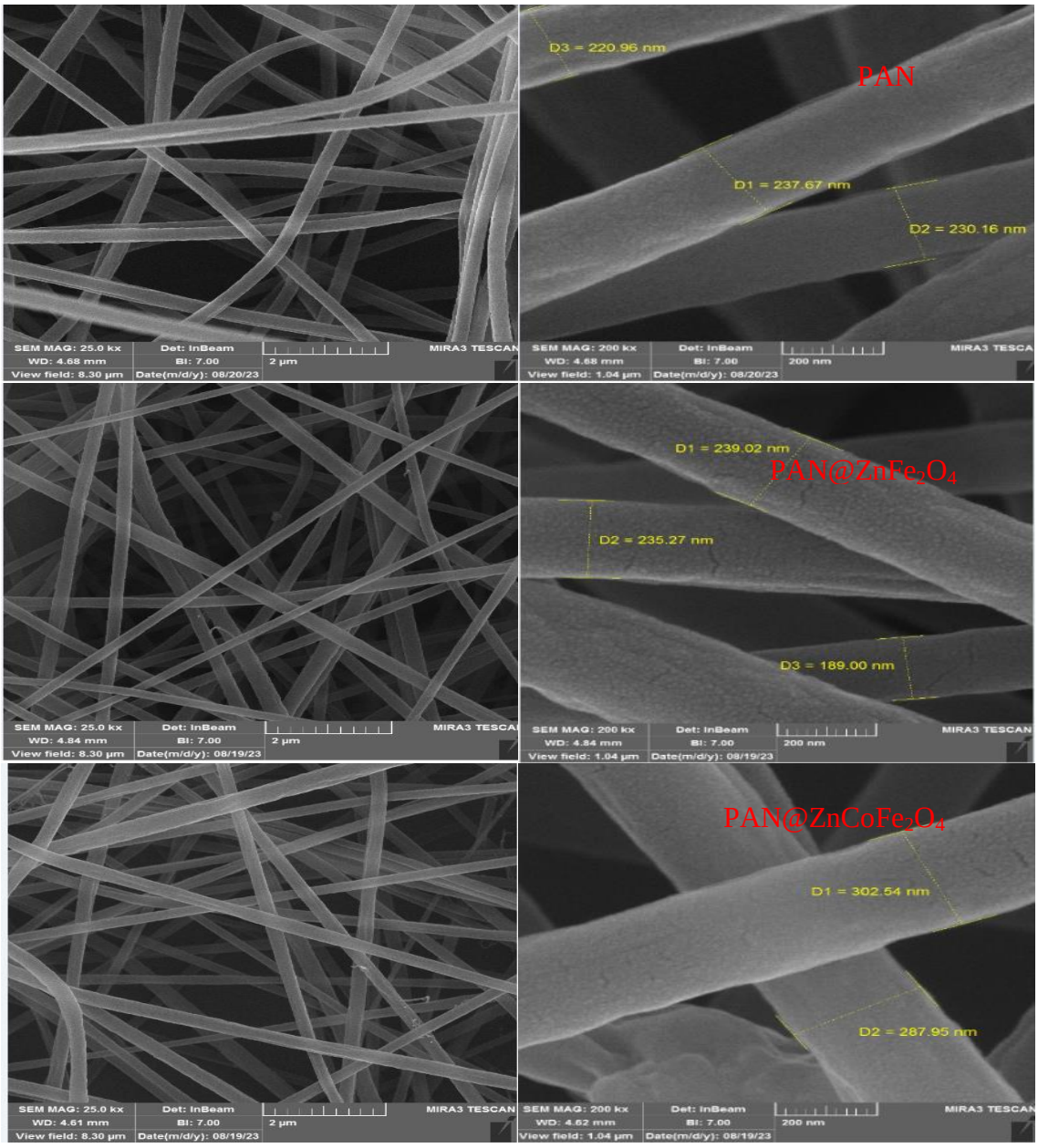

Figure 3: FESEM images of PAN and PAN@Ferrites composites.

Fourier transformer infrared (FTIR) examination of vibration modes is shown in Fig. 4. In addition to a high absorption from 1033 to 1253 cm^{-1}, the $ZnFe_2O_4$ also showed an extra absorption at 647 cm^{-1}. Typically, the showed an absorption from 1385 to 478cm^{-1}. These absorptions show that compounds or elements have stretching vibrations between metal and oxygen. In addition, absorption took place at 1756, 2264, and 1463 cm^{-1}, which are the O-H stretches that normally extend from 1385 to 1637 cm^{-1}. By extending the vibrations of C-H at 2977 cm^{-1}, which goes from 2922 to

3426 cm^{-1}, and O-H at 3433 cm^{-1}, which typically goes from 3426 to 3779 cm^{-1}, compounds or components absorb light.

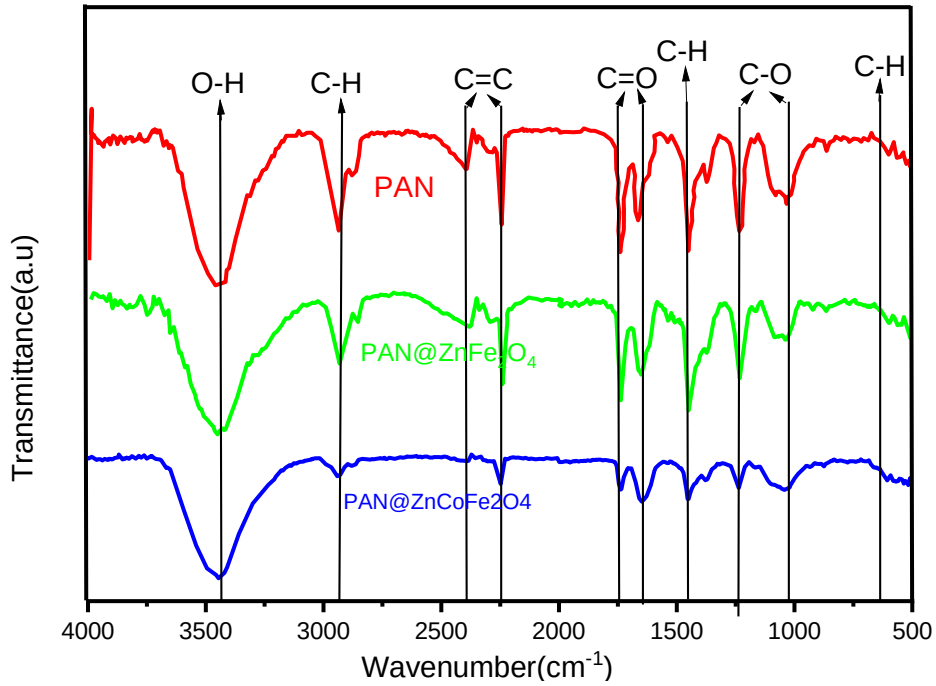

Figure 4: FTIR spectra of PAN NFs and its composites with ferrite.

The current-voltage characteristics of pure PAN NFs and fertilized PAN NFs composites are shown in Fig. 5. I-V characteristic curve for pure PAN, PAN@$ZnFe_2O_4$ and PAN@$ZnCoFe_2O_4$ NFs exhibit Schottky behavior. The current flow between electrodes usually increases with high bias voltages and decreases with low voltages. Reverse behavior is defined by a reduced current at reverse bias levels in contrast to forward bias levels, as seen in Figs. 5b and c. This effect may arise from adding ferrites to PAN lattices, as the structure gets distorted by the enormous radius of the zinc, iron, and cobalt cations. Due to reverse biasing, the electrons and holes move away from the junction region, increasing the depletion area and raising the voltage value.

The influence of humidity on the electrical characteristics was examined through the measurement of resistance under applied voltage. The Instek 6100 LCR meter is utilized to quantify the resistance R of samples. The experimental configuration for assessing the resistance of the humidity sensor employed a regulated humidity room fitted with inlet and exit valves for vapor circulation. A commercial humidity meter (Testo 625 Thermo Hygrometer) was utilized to monitor humidity levels during the resistance tests. The humidity was controlled by modulating humid air, enabling accurate regulation of the relative humidity (RH) within the chamber. The system achieved a broad spectrum of humidity values, ranging from 50% to 100% RH, by adjusting the flow rates of wet.

Humidity sensor combines a thin-layered from PAN and its composites with ferrites which is sensitive material and changes their electrical properties (resistance or capacitance) as they absorb moisture from the surrounding environment. In our case, we study the resistance. Also, aluminum electrodes for measurement, deposited on nano fibers and these layers are deposited on Si substrate for structural support. The performance of the sensor depends on the material's ability to change electrical properties in response to humidity variations, with the thin film enhancing the sensor's sensitivity and response time. Fig. 6 demonstrate a positive correlation between

resistance (R) and relative humidity (RH), demonstrating that the materials grow more resistant as the humidity increases.

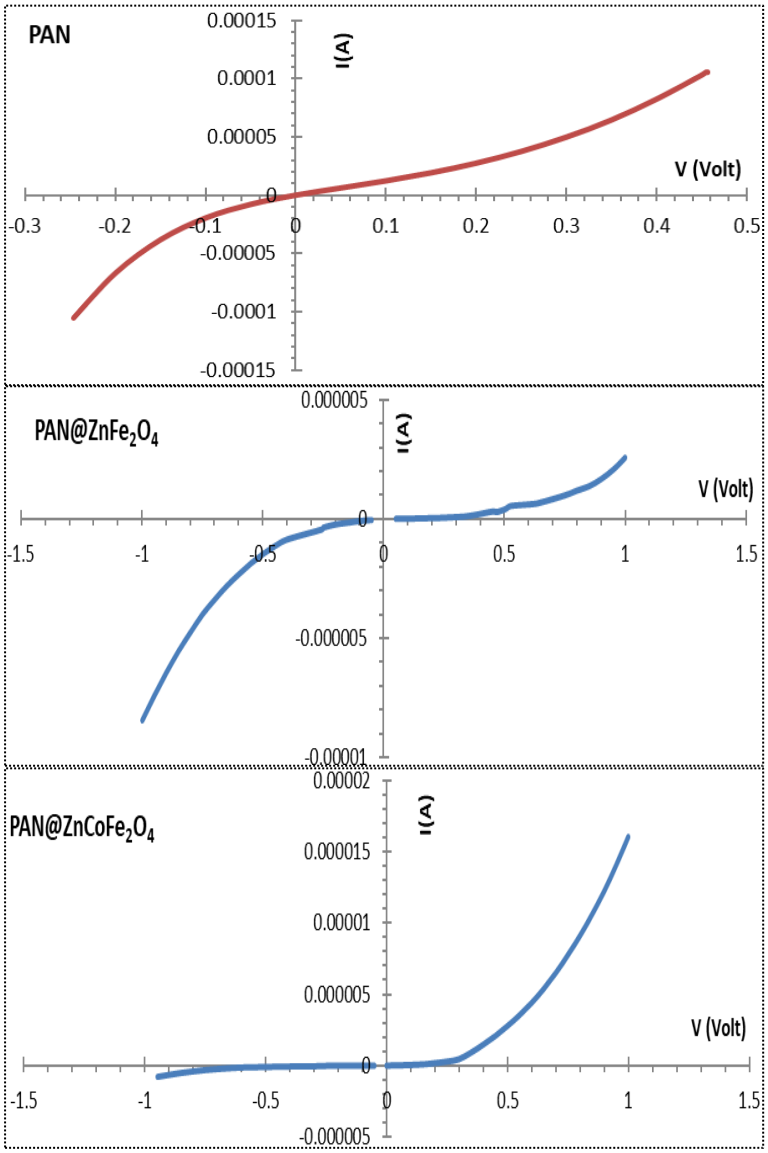

Figure 5: Current-Voltage comparison between dark and light for PAN, PAN@$ZnFe_2O_4$ and PAN @$ZnCoFe_2O_4$ NFs.

For PAN NFs, there is no effect when relative humidity percentage increases and decreases but with adding ferrite materials such as PAN@$ZnFe_2O_4$ and PAN@$ZnCoFe_2O_4$ where there is significant change in resistance when humidity increases and decreases as shown in Fig. 6. The material containing pure PAN exhibits constant resistance across the whole range of relative humidity, whereas PAN@$ZnCoFe_2O_4$ demonstrates the highest resistance change. These findings indicate that the addition of ferrite material improves the conductivity of the composite, hence increasing its sensitivity to changes in humidity.

Clusters of water molecules were detected, which directly influenced the performance of the resistive-type sensors utilized in this work. The sensor's resistance varied in direct correlation to the extent of water molecule aggregation [30]. The resistance of the sensor did not increase much as the relative humidity increased from 50% to 100%, suggesting that the dielectric constant was not significantly influenced by the water molecules adsorbed in the first layer. This is because, in the presence of an

externally imposed electric field, the hydrogen bonding between. The chemisorbed water molecules on the composite nanofiber surface impede their capacity for free alignment. Consequently [31]. The resistance markedly escalates around 60% relative humidity. This behavior indicates that at roughly 50% relative humidity, the initial layer of chemisorbed water is nearly complete, and the formation of the second layer of water adsorption is commencing. The creation of extra water layers can impede charge transmission, leading to a significant increase in resistance at elevated humidity levels. The sensing material's multilayer development causes a notable increase in capacitance and resistance between 50% and 90% RH. By measuring the capacitance and resistance responses of the composite nanofibers as a function of frequency at different relative humidity levels, the efficacy of the nanofibers' humidity sensing system was examined. Based on early investigations, the composite nanofibers had a strong resistance response. The study demonstrates that the capacitance and resistance of the sensor rose significantly when the relative humidity value was changed. The water molecules that stick to the sensor's surface are directly influenced by the relative humidity, which causes a notable rise in capacitance throughout the adsorption process. When there is low humidity and minimal water absorption, the sensor material is in its ideal location.

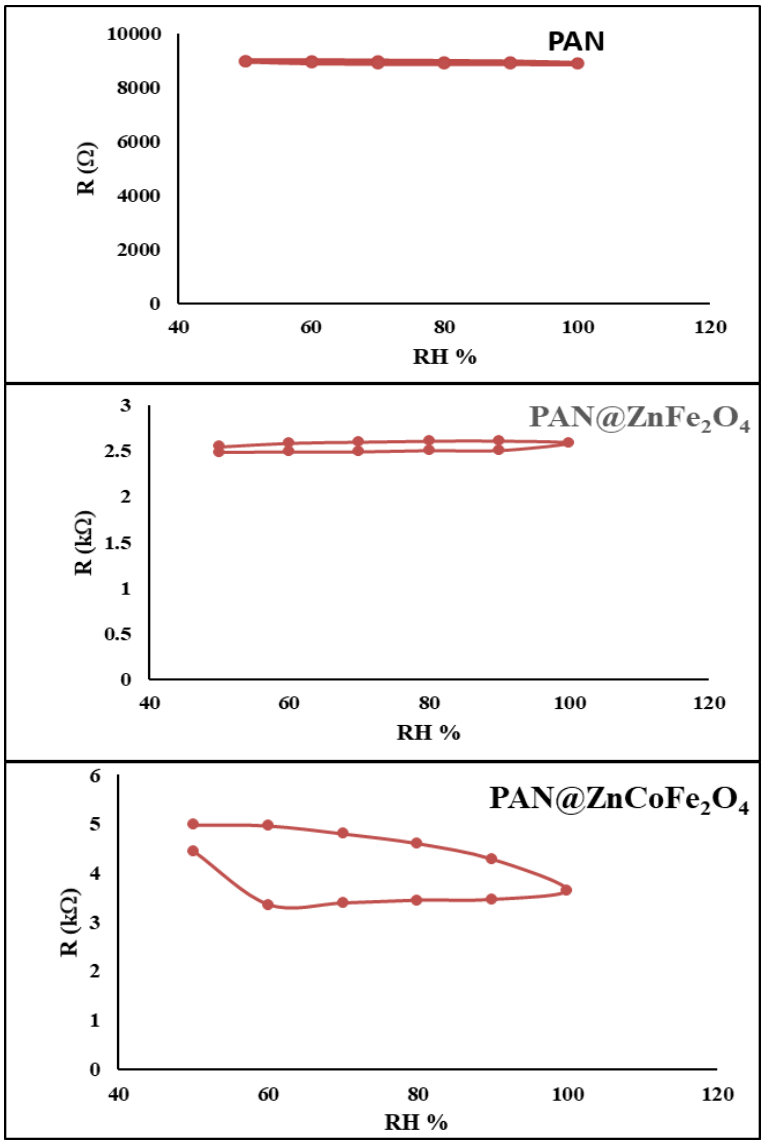

Figure 6: Humidity sensor of PAN, PAN @ $ZnFe_2O_4$ and PAN@$ZnCoFe_2O_4$ composite.

4. Conclusions

PAN@$ZnFe_2O_4$ was successfully synthesized by electrospinning, and the characteristic nanosized crystal structure is represented by the broad peak in the X-ray diffraction study. Switching devices utilise the non-ohmic properties of these nanofibers, which exhibit a rectifying characteristic, allowing for the regulation of current flow in a single direction, which is shown by current-voltage characterisation. Because of their hydrophilicity, these nano fibres are suitable for humidity sensors.

References

1. H. R. Darrell and C. Iksoo, Nanotechnology **7**, 216 (1996). DOI: 10.1088/0957-4484/7/3/009.
2. J. Ding, J. Zhang, J. Li, D. Li, C. Xiao, H. Xiao, H. Yang, X. Zhuang, and X. Chen, Prog. Poly. Sci. **90**, 1 (2019). DOI: 10.1016/j.progpolymsci.2019.01.002.
3. L. Liu, W. Xu, Y. Ding, S. Agarwal, A. Greiner, and G. Duan, Comp. Commun. **22**, 100506 (2020). DOI: 10.1016/j.coco.2020.100506.
4. T. Senthil Muthu Kumar, K. Senthil Kumar, N. Rajini, S. Siengchin, N. Ayrilmis, and A. Varada Rajulu, Comp. Part B Eng. **175**, 107074 (2019). DOI: 10.1016/j.compositesb.2019.107074.
5. J. Xue, T. Wu, Y. Dai, and Y. Xia, Chem. Rev. **119**, 5298 (2019). DOI: 10.1021/acs.chemrev.8b00593.
6. I. Moulefera, M. Trabelsi, A. Mamun, and L. Sabantina, Polymers **13**, 1071 (2021). DOI: 10.3390/polym13071071.
7. L. Zhang, A. Aboagye, A. Kelkar, C. Lai, and H. Fong, J. Mat. Sci. **49**, 463 (2014). DOI: 10.1007/s10853-013-7705-y.
8. R. Awad, A. Haghighat Mamaghani, Y. Boluk, and Z. Hashisho, Chem. Eng. J. **410**, 128412 (2021). DOI: 10.1016/j.cej.2021.128412.
9. L. Veeramuthu, M. Venkatesan, F.-C. Liang, J.-S. Benas, C.-J. Cho, C.-W. Chen, Y. Zhou, R.-H. Lee, and C.-C. Kuo, Polymers **12**, 587 (2020). DOI: 10.3390/polym12030587.
10. A. Salam, T. Hassan, T. Jabri, S. Riaz, A. Khan, K. M. Iqbal, S. U. Khan, M. Wasim, M. R. Shah, M. Q. Khan, and I.-S. Kim, Nanomaterials **11**, 2208 (2021). DOI: 10.3390/nano11092208.
11. N. Ucar, N. Kizildag, A. Onen, I. Karacan, and O. Eren, Fib. Poly. **16**, 2223 (2015). DOI: 10.1007/s12221-015-5426-3.
12. J.-S. Tsai and C.-H. Lin, J. Appl. Polym. Sci. **42**, 3045 (1991). DOI: 10.1002/app.1991.070421124.
13. G. Duan, S. Liu, and H. Hou, e-Polymers **18**, 569 (2018). DOI: 10.1515/epoly-2018-0158.
14. G. K. Celep and K. Dincer, Int. Poly. Proc. **32**, 508 (2017). DOI: 10.3139/217.3411.
15. L. L. Beecroft and C. K. Ober, Chem. Mat. **9**, 1302 (1997). DOI: 10.1021/cm960441a.
16. D. Chavez, J. Angel, and D. Burke. *Energy Transition or Energy Expansion?*, The Transnational Institute (TNI) and Trade Unions for Energy Democracy (TUED) https://www.tni.org/en/publication/energy-transition-or-energy-expansion.
17. G. Mo, R. Zhang, Y. Wang, and Q. Yan, Polymer **84**, 243 (2016). DOI: 10.1016/j.polymer.2016.01.002.
18. J. Sun, H. R. Jiang, M. C. Wu, X. Z. Fan, C. Y. H. Chao, and T. S. Zhao, J. Pow. Sour. **470**, 228441 (2020). DOI: 10.1016/j.jpowsour.2020.228441.
19. M. H. Feng and X. J. Li, Sens. Actuat. B Chem. **272**, 543 (2018). DOI: 10.1016/j.snb.2018.06.023.
20. M. T. S. Chani, K. S. Karimov, S. B. Khan, N. Fatima, and A. M. Asiri, Ceram. Int. **45**, 10565 (2019). DOI: 10.1016/j.ceramint.2019.02.122.
21. P. Li, X. Zheng, Y. Zhang, M. Yuan, B. Jiang, and S. Deng, Ceram. Int. **41**, 14251 (2015). DOI: 10.1016/j.ceramint.2015.07.054.
22. Z. Imran, S. S. Batool, H. Jamil, M. Usman, M. Israr-Qadir, S. H. Shah, S. Jamil-Rana, M. A. Rafiq, M. M. Hasan, and M. Willander, Ceram. Int. **39**, 457 (2013). DOI: 10.1016/j.ceramint.2012.06.048.
23. J. Bhadra, A. Popelka, A. Abdulkareem, M. Lehocky, P. Humpolicek, and N. Al-Thani, Sens. Actuat. A Phys. **288**, 47 (2019). DOI: 10.1016/j.sna.2019.01.012.
24. S. Mallick, Z. Ahmad, F. Touati, and R. A. Shakoor, Sens. Actuat. B Chem. **288**, 408 (2019). DOI: 10.1016/j.snb.2019.03.034.
25. D. Zhang, M. Wang, and Z. Yang, Sens. Actuat. B Chem. **292**, 187 (2019). DOI: 10.1016/j.snb.2019.04.133.
26. H. M. Hawy and I. M. Ali, Optik **267**, 169659 (2022). DOI: 10.1016/j.ijleo.2022.169659.
27. K. Raja, C. Prabhu, K. S. Subramanian, and K. Govindaraju, Poly. Bull. **78**, 6429 (2021). DOI: 10.1007/s00289-020-03435-6.
28. I. K. Abd Karem and S. A. Hamdan, Iraqi J. Sci. **63**, 2482 (2022). DOI: 10.24996/ijs.2022.63.6.15.
29. S. A. Hamdan, I. M. Ibrahim, and I. M. Ali, J. Phys. Conf. Ser. **2114**, 012025 (2021). DOI: 10.1088/1742-6596/2114/1/012025.

30. D. M. Dabbs and I. A. Aksay, Ann. Rev. Phys. Chem. **51**, 601 (2000). DOI: 10.1146/annurev.physchem.51.1.601.
31. M. Backman, N. Juslin, and K. Nordlund, Eur. Phys. J. B **85**, 317 (2012). DOI: 10.1140/epjb/e2012-30429-y.

ألياف نانوية من مادة PAN@Ferrites المصنوعة بالغزل الكهربائي لأجهزة التقويم والرطوبة

بان عباس رجه[1] و افتخار محمود علي[1]
[1]قسم الفيزياء، كلية العلوم، جامعة بغداد، بغداد، العراق

الخلاصة

تم تحضير فيريت الزنك والكوبالت ($ZnCoFe_2O_4$) وفيريت الزنك ($ZnFe_2O_4$) باستخدام تخليق السول-جل. تم إنشاء المواد المركبة، $PAN@CoFe_2O_4$ و $PAN@ZnCoFe_2O_4$، من خلال الجمع بين بوليمر بولي أكريلونيتريل (PAN) مع $ZnCoFe_2O_4$ و $ZnFe_2O_4$. تم استخدام الغزل الكهربائي لتطبيق الطلاءات الرقيقة على الزجاج ورقائق p-Si. تم توضيح الألياف المصنعة لكل من بوليمرات PAN النقية والمركبات القائمة على الفريت في صور المجهر الإلكتروني الماسح للانبعاث الميداني (FESEM). يكشف تحليل حيود الأشعة السينية (XRD) أن بوليمر PAN يُظهر ذروة بارزة بزاوية دقيقة تبلغ 29. 3345 درجة. يظل حجم هذه الذروة ثابتًا في مركبات PAN التي تحتوي على $ZnCoFe_2O_4$ و $CoFe_2O_4$. يُظهر محول فورييه بالأشعة تحت الحمراء (FTIR) أن الامتصاصات لها اهتزازات تمدد بين المعدن والأكسجين. تُظهر مركبات الألياف النانوية خصائص غير أومية، كما يتضح من اختبارات التيار والجهد (I-V). تُظهر ألياف النانو PAN خصائص موصلة، بينما تُظهر مركبات الفريت الخاصة بها سلوك تصحيح في درجة حرارة الغرفة عند تعرضها لحقل منخفض التطبيق. بالنسبة لألياف PAN NFs، لا يوجد تأثير عندما تزيد وتنخفض نسبة الرطوبة النسبية، ولكن مع إضافة مواد الفريت $PAN@ZnFe_2O_4$ و $PAN@ZnCoFe_2O_4$، يوجد تغيير كبير في المقاومة عندما تزيد وتنخفض الرطوبة.

الكلمات المفتاحية: متحسس الرطوبة، الياف اكريلونيتريل النانويه، حديديت الكوبلت والزنك، حديديت الزنك، الغزل الكهربائي.